Acupuncture and Herbal Medicine

The *Hemerocallis citrina* extracts ameliorate radiation-induced ferroptosis in LO2 cells through the Nrf2-xCT/GPX4 pathway

Zihao Zhu, Yan Wang, Zhengzheng Deng, Pengyuan Lei, Qi Liu, Jinjing Guo, Qiancheng Qing, Bo Huang*

College of Public Health, Hengyang Medical School, University of South China, Hengyang, China

Abstract

Background: Radiotherapy, a primary approach in cancer treatment, damages normal cells while targeting cancer cells. Therefore, it is crucial to identify drugs with minimal side effects, high reliability, and radioprotective effects to develop novel radiotherapy strategies. *Hemerocallis citrina* extracts (HCE), which are derived from plants with medicinal and culinary applications, possess antioxidative and anticancer properties.

Methods: In this study, we investigated the radioprotective effects of HCE on LO2 cells exposed to radiation to determine whether these effects were mediated through the nuclear factor erythroid 2–related factor 2-cystine–glutamate antiporter/glutathione peroxidase 4 pathway.

Results: Cell proliferation experiments demonstrated the radioprotective effect of HCE on LO2 cells. Western blot analysis revealed that HCE regulated B-cell lymphoma protein 2-associated X, Cleaved-caspase 3, and B-cell lymphoma protein 2, thereby inhibiting radiation-induced apoptosis, which was consistent with the flow cytometry results.

Conclusions: Moreover, the detection of ferroptosis-related markers indicated that HCE alleviated radiation-induced ferroptosis in LO2 cells through the nuclear factor erythroid 2–related factor 2-cystine–glutamate antiporter/glutathione peroxidase 4 pathway. These findings provide a theoretical basis for the radioprotective effects of HCE on LO2 cells and offer new insights into the development of radioprotective drugs.

Keywords: Ferroptosis, *Hemerocallis citrina* extract, Nrf2-xCT/GPX4 pathway, Radioprotection

Graphical abstract: http://links.lww.com/AHM/A122.

Introduction

Ionizing radiation (IR) is emitted during the ionization process of matter and encompasses high-energy electromagnetic waves such as X and γ-rays, fast-charged particles such as α and β particles, and neutral particles like neutrons[1]. IR has been widely used in various fields, with the highest utilization in the medical sector. With the rapid development of nuclear technology, the risks associated with exposure to IR are increasing, emphasizing the need for radiation protectants or therapeutic agents. Exposure to IR can cause acute or chronic damage to various systems in the human body[2–4].

Liver cancer, which is characterized by high mortality and morbidity, is commonly treated with radiotherapy, a modality that triggers cancer cell death through IR. The liver, a radiation-sensitive organ, ranks second only to the bone marrow, lymph nodes, gastrointestinal tract, gonads, embryos, and kidneys in terms of susceptibility to radiation[5]. The protection of normal cells has become a focal point in radiotherapy research. IR can induce various forms of cell death, including apoptosis, necrosis, ferroptosis, pyroptosis, and autophagy. Apoptosis is the primary pathway of radiation-induced cell damage caused by radiation[6]. In addition to apoptosis, other forms of cell death, such as ferroptosis, necroptosis, and autophagy, have been found to be involved in cell death induced by radiotherapy[7]. Ferroptosis is a distinct type of cell death regulated by iron ions and exhibits morphological, biochemical, and genetic differences from apoptosis, autophagy, and necrosis[8,9]. Ferroptosis plays a crucial role in the development of various diseases, including cancer, neurological disorders, and ischemic injuries[10,11]. In recent years, researchers have discovered the pivotal mechanism of ferroptosis in mediating cell death induced by radiotherapy, suggesting new strategies for enhancing radiotherapy sensitivity and

Zihao Zhu and Yan Wang contributed equally to this work.

**Corresponding author: Bo Huang, E-mail: huangbo0930@163.com.*

Received 30 January 2024 / Accepted 6 June 2024

How to cite this article: *Zhu ZH, Wang Y, Deng ZZ, Lei PY, Liu Q, Guo JJ, Qing QC, Huang B. The Hemerocallis citrina extracts ameliorate radiation-induced ferroptosis in LO2 cells through the Nrf2-xCT/GPX4 pathway. Acupunct Herb Med 2024;4(4):513–524. DOI: 10.1097/HM9.0000000000000120*

protecting against radiation damage by regulating and intervening in tumor cell ferroptosis[12].

Despite a deeper understanding of the mechanisms of IR-induced tissue damage, the number of Food and Drug Administration-approved radiation protectants and therapeutic drugs remains limited. Therefore, it is essential to explore new radiation protectants that have fewer side effects and are effective in their actions. Plant-derived natural compounds with advantages such as broad efficacy, minimal toxicity, convenient administration, low cost, and patient acceptance represent highly promising avenues for the development of radiation protectants or therapeutic drugs[13]. Numerous studies have indicated that various active components of traditional Chinese medicines exhibit radioprotective effects, including polysaccharides, alkaloids, and polyphenols[14,15]. Flavonoids are among the most important biologically active compounds in herbal medicines. Currently, flavonoids such as total flavones from Astragalus membranaceus, icariin, total flavones from Herba Epimedii, genistein, quercetin, and apigenin have been discovered to exhibit excellent radioprotective effects on the hematopoietic system, immune system, reproductive system, or skin[16–18]. Therefore, the active flavonoid ingredients in traditional Chinese medicine may represent potential radioprotective drugs.

Hemerocallis citrina (Huanghua Cai) belongs to the Asteraceae family, and its leaves, which are a common vegetable in China, are nutritionally rich. *Hemerocallis citrina* extracts (HCE) contain various bioactive substances, such as proteins, carbohydrates, vitamins, polyphenols, terpenes, anthraquinones, saponins, and alkaloids. With properties including calming, hemostasis, anti-inflammatory, antioxidant, digestion-promoting, heat-clearing, and antidepressant effects, it has been widely used in clinical settings for treating conditions like cancer, jaundice, edema, and bloody stools, with a long history of use[19–21].

Pharmacological studies of this plant genus have resulted in the isolation of flavonoids, polysaccharides, alkaloids, and terpenoids, which show a wide range of activities, including anticancer, neuroprotective, hepatoprotective, and antiproliferative effects. Thus, HCE have medicinal and dietary applications. Previous studies have reported the anticancer activity of HCE; however, studies on its radioprotective properties are limited.

Nuclear factor erythroid 2–related factor 2 (Nrf2) is a crucial transcription factor first isolated and identified by Moi et al.[22]. Nrf2 belongs to the cap'n'collar subfamily of transcription factors and is widely expressed in all tissues, albeit at a relatively low baseline level[23]. Under normal cellular conditions, Nrf2 binds to Kelch-like ECH-associated protein 1 and remains inactive, continuously undergoing ubiquitination and degradation in the proteasome[24]. Nrf2 regulates numerous target genes, including the intracellular redox balance proteins hematopoietic protein 1 and glutathione peroxidase (GPX), phase II detoxifying enzymes glutathione S-transferase and NAD(P)H quinone oxidoreductase (NQO-1), and multidrug resistance–associated proteins[25]. These downstream effectors play crucial roles in the cellular defense mechanisms. Therefore, Nrf2 is a key factor that protects cells from the effects of oxidation.

Cystine–glutamate antiporter (xCT), which is associated with cellular protection, is a key gene regulated by Nrf2[26]. xCT (also known as SLC7A11) forms a cystine–glutamate antiporter system along with CD98, facilitating the exchange of glutamate out of the cell and cysteine into the cell at a 1:1 ratio[27]. Within the cell, cysteine is converted to cysteamine, a limiting amino acid essential for the production of the cytoprotective agent glutathione (GSH). Additionally, xCT is an important factor in the cellular antioxidant system playing[28].

In this study, we used LO2 cells as a model to investigate radiation damage. We performed extracellular analyses to investigate the effects of HCE through the Nrf2-xCT/GPX4 pathway on IR-induced damage in normal human liver cells. We also explored the potential mechanisms underlying the radioprotective effects of HCE.

Materials and methods

Preparations of HCE

HCE were obtained from Nanjing Zelang Medical Technology, China, and were prepared using the flowers of *H. citrina*. First, 250 g of chopped dried flowers was extracted twice with 2.5 L of 90% ethanol for 2 h and then 1.5 L with 70% ethanol for 1 h. The extracts were mixed, filtered to remove the impurities, and concentrated under reduced pressure. Next, the concentrate was concentrated to 500 mL with distilled water and loaded onto a macroporous adsorbent resin column. The resulting samples were first eluted with water and then with different concentrations (10%, 30%, and 50%) of ethanol. Each eluate was separately compressed under reduced pressure and lyophilized for storage. Lyophilized powders at different concentrations were eluted with ethanol to obtain HCE[29]. The extracts were eluted with 50% ethanol.

Cell culture and irradiation conditions

LO2 cells were cultured in 1640 RPMI basal medium supplemented with 10% fetal bovine serum and 1% antibiotics (containing 11.11 mmol/L glucose) at 37°C in a 5% CO_2 incubator. The medium was refreshed every 1 to 2 days. LO2 cells were irradiated with 8 Gy of γ-rays using a 137Cs biological irradiator (HXFS-IA, China) at a rate of 120 cGy/min. The experiments were conducted 24 h after irradiation. For specific experimental groups, HCE dissolved in dimethyl sulfoxide (DMSO) at a concentration of 98% were added to LO2 cells 6 h prior to irradiation.

Cell grouping

LO2 cells were randomly divided into the following groups: negative control (NC) group, HCE treatment group without irradiation (HCE), IR, irradiation with HCE treatment group (HCE + IR), irradiation with ferroptosis inhibitor group (FER-1 + IR), irradiation with Nrf2 inhibitor group (IR + ML + 385), and irradiation with HCE and Nrf2 inhibitor group (IR + HCE + ML385).

Cell proliferation and clonogenic assays

3-(4,5-dimethylthiazol-2-yl)-2,5-diphenyltetrazolium bromide (MTT) assay for cell viability

LO2 cells were seeded in 96-well plates at a density of 5.0×10^3 cells/mL. After incubating for 24, 48, and 72 h, 10 µL of MTT and 90 µL of medium were added to each well. The incubation process was continued at 37°C for 4 h. After removing the supernatant, 110 µL of formazan solution was added to each well, and the plate was oscillated for 10 min. Absorbance was measured at 490 nm using an enzyme-linked immunosorbent assay reader, and cell viability was analyzed.

The formula for calculating viability was as follows:

$$\text{Viability} = \frac{\text{Average absorbance value (OD) of the experimental group}}{\text{Average absorbance value (OD) of the control group}} \times 100\%$$

Growth curve experiment for cell growth and viability

LO2 cells were seeded in a 96-well plate at a density of 5.0×10^3 cells/mL and incubated in a 37°C constant temperature incubator. Each group consisted of three parallel samples, and cell counting was performed every 24 h over a continuous 7-day period.

Colony formation assay for observation of cellular colony-forming ability

LO2 cells in the logarithmic growth phase were seeded in six-well plates at a density of 600 cells/mL, with 1 mL per well. At least three replicate wells were prepared for each group, and the culture medium was refreshed every 3 days. After 10 days of incubation, the culture was terminated. The cells were gently washed two to three times with phosphate-buffered saline (PBS), fixed with 4% paraformaldehyde for 30 min, and stained with an appropriate amount of diluted Giemsa solution for 30 min. The staining solution was gently washed with running water, and the plate was naturally inverted to air-dry. Clones containing more than 50 cells were counted. The formula for calculating the colony formation rate was as follows:

$$\text{Cell attachment rate } (\%) = \frac{\text{number of clones in the untreated group}}{\text{number of cells seeded in the untreated group}} \times 100\%$$

$$\text{Cell survival fraction } (\%) = \frac{\text{number of clones}}{\text{number of cells seeded in the treatment group}} \times \text{cell attachment rate} \times 100\%$$

Detection of changes in antioxidant indices levels (superoxide dismutase (SOD), GSH, malondialdehyde (MDA)) in cells

After a 24-hour period of cell culture, the culture medium was aspirated, and the cells were harvested through trypsin digestion. The cells were then washed twice with PBS. Subsequently, 80 µL of cell lysis buffer (Baiyuntian Biotechnology, Shanghai, China) was added to each well, followed by an incubation period of 1 h. The supernatant was collected by centrifuging at 4°C and 12,000 rpm for 15 min. The total protein concentration in each well was determined using a bicinchoninic acid (BCA) Protein Assay Kit (Conway Institute of Biomedical and Biomolecular Research, Dublin, Ireland). MDA, SOD, and GSH levels were quantified using specific assay kits.

Detection of intracellular reactive oxygen species (ROS) levels

LO2 cells in the logarithmic growth phase were seeded in six-well plates at a density of 5.0×10^4 cells/mL, with 2 mL per well. After 24 h of incubation, the culture medium was discarded, and the cells were washed twice with PBS. Each well was then treated with 1 mL of 10 µmol/mL DCFH-DA fluorescence probe culture medium and incubated at 37°C for 30 to 60 min. After washing twice with PBS at 4°C, trypsin digestion was performed, and cells were resuspended and centrifuged at 5,000 rpm for 5 min. The supernatant was discarded, and the cells were collected. After adding 1 mL of PBS and resuspending, centrifugation at 4°C was performed for one to two rounds. The supernatant was discarded, and each well was treated with 500 µL of PBS. A fluorescence spectrophotometer was used to measure the ROS content in each group, with the optimal excitation wavelength set at 485 nm and emission wavelength set at 525 nm.

Cell apoptosis and cycle

Flow cytometry assay for cell apoptosis rate

LO2 cells in the logarithmic growth phase were seeded in six-well plates at a density of 5.0×10^4 cells/mL, with 2 mL per well. After 24 h of incubation, the culture medium was discarded, and the cells were harvested following trypsin digestion. After centrifuging to remove the supernatant, cells were suspended in 100 µL of binding Buffer. Subsequently, a mixture of 5 µL of Annexin V-fluorescein isothiocyanate (FITC) and 5 µL of propidium iodide was added, and the cells were incubated for 5 min. Finally, 400 µL of binding buffer was added and mixed. The reaction was conducted in the dark on a clean bench for 5 to 15 min and then analyzed using a flow cytometer within 1 h.

Flow cytometry assay for cell cycle

After appropriate treatment, the cells were cultured for 24 h, and then the samples were collected. The cells were gently washed once with PBS and centrifuged at 2,000 rpm for 5 min. Before staining, the 70% ethanol fixative was washed twice with 1 mL of PBS, and the cell pellet was collected by centrifuging at 1,000 rpm for 5 min. The cells were then stained with 500 µL of PI/RNaseA staining working solution (RnaseA:PI = 1:9) at room temperature in the dark for 30 to 60 min, and the cell cycle was analyzed using a flow cytometer.

Rhodamine probe to measure changes in cell mitochondrial membrane potential

LO2 cells in the logarithmic growth phase were seeded in six-well plates at a density of 5.0×10^4 cells/mL, with 2 mL per well. After 24 h of incubation, the culture medium was discarded based on the radiation bystander effect model. The cells were washed two to three times with Dulbecco's PBS (DPBS), trypsinized, and collected. The cells were resuspended in 1 mL of DPBS at 4°C, and then 1 µL of Rhodamine B was added to each tube to achieve a final concentration of 100 µg/mL. After incubation in the dark for 0.5 h, the cells were centrifuged at 9,000 rpm for 3 min to collect the cell pellet. The cells were resuspended in 1 mL of DPBS per tube, and the mitochondrial membrane potential of each group was measured using a fluorescence spectrophotometer (optimal excitation wavelength of 488 nm and emission wavelength of 525 nm).

Detection of cellular ferrous ion concentration

First, 2 µL of the standard solution with 198 µL of deionized water were mixed to prepare a 1 mM iron standard solution. The iron standard solution was diluted with the assay buffer and added to a 96-well plate at concentrations of 0, 2, 4, 6, 8, and 10 nmol/well. Then, 5 µL of iron reducer was added to each well and incubated at 37°C for 30 min. Subsequently, 100 µL of the probe was added to each well and incubated at 37°C in the dark for 60 min. LO2 cells were collected in the logarithmic growth phase from each experimental group using ethylenediaminetetraacetic acid-free trypsin and resuspended in 5 mL of culture medium. Next, 0.5 mL was collected for protein detection, and protein concentration was determined using the BCA method. The remaining 4.5 mL was centrifuged at 1,000 rpm for 5 min to remove the supernatant. Then, 100 µL of assay buffer was added to resuspend the cells. The solution was vortexed for 20 seconds, placed in a −80°C freezer for 10 min, and warmed to 37°C in a water bath, and this process was repeated three times. It was centrifuged at 2,000×*g* for 5 min. The supernatant was collected for further analysis. In each well of a 96-well plate, 100 µL of the tested supernatant and 5 µL of assay buffer were added and incubated at 37°C for 30 min. Then, 100 µL of the probe was added to each well and incubated at 37°C in the dark for 60 min. After incubation, the absorbance (optical density [OD]) was measured at 593 nm using a microplate reader, and a standard curve of the iron concentration against the OD values was plotted.

LO2 cells in the logarithmic growth phase were divided into four groups: blank control (NC), drug-treated (HCE), IR, and irradiation + 200 µg/mL HCE (HCE + IR), based on a cell density of 5.0×10^4 cells/mL, and then seeded into six-well plates. Each group had a minimum of three replicate wells. After 24 h of incubation, the culture medium was aspirated, and the cells were rinsed with PBS. Subsequently, 200 µL of 1 µmol/L Liperfluo solution, diluted in serum-free DMEM medium, was added to each well of the six-well plates, and the cells were then incubated in a 37°C 5% CO_2 atmosphere for 30 min. The medium was aspirated, and the cells were washed twice with PBS before observation under a fluorescence microscope.

Detection of intracellular lipid peroxidation

First, 1 mg of C11 Bodipy powder was dissolved in 198.25 µL of DMSO to prepare a solution with a concentration of 10 mmol/mL. LO2 cells were seeded in the logarithmic growth phase in a six-well plate after transfection and cultured overnight. A specific drug/irradiation dose was administered to the cells, and cells were cultured for a defined duration. The original culture medium was removed and replaced with 10 µmol/mL C11 Bodipy-containing culture medium for the staining group, followed by incubation for 30 min. The culture medium was removed, and the cells were rinsed three times with PBS. The cells were digested with trypsin and centrifuged at 2,000 rpm for 3 min. The supernatant was discarded, and the cells were resuspended in 1 mL of PBS. It was centrifuged at 4,000 rpm for 3 min, and the washing step was repeated three times with PBS. The cells were resuspended in 1 mL of PBS and analyzed using a flow cytometer.

Western blot detection of protein expression

LO2 cells in the logarithmic growth phase were seeded at a density of 4.0×10^6 cells/mL in 6-cm flat dishes, with 2 mL per dish, and harvested after 24 h. Following treatment, the Total Protein Extraction Kit (Baiyuntian Biotechnology) was used to extract total protein according to the manufacturer's instructions. The BCA Protein Assay Kit was used to determine the protein concentration. Samples were processed on sodium dodecyl-sulfate-polyacrylamide gel electrophoresis gels, and proteins were transferred from the gels to polyvinylidene difluoride membranes (Solarbio, Beijing, China). The membranes were subsequently incubated in Tris buffered saline with Tween 20 (TBST) (20 mmol/L Tris, 500 mmol/L NaCl, and 0.1% Tween-20) containing 5% skim milk powder for 2 h and then rinsed three times with TBST for 10 min each time. The membranes were incubated with the primary antibody at 4°C overnight, then washed three times with TBST for 15 min each time, and incubated with the secondary antibody in TBST for 1 h at room temperature. Western blots were densitometrically analyzed using ImageJ.

Statistical analysis

All data were analyzed using SPSS 25.0 and presented as the mean ± standard deviation. One-way analysis of variance was used to assess differences among groups, and *post hoc* multiple comparisons were conducted using the Student-Newman-Keuls test. Statistical significance was set at $P < 0.05$.

Results

Impact of HCE on cell proliferation

Figure 1A shows that the MTT assay revealed a significant decrease in the cell survival rate with increasing radiation intensity. Additionally, the HCE group showed slightly higher cell survival rates than the NC group. Figure 1B

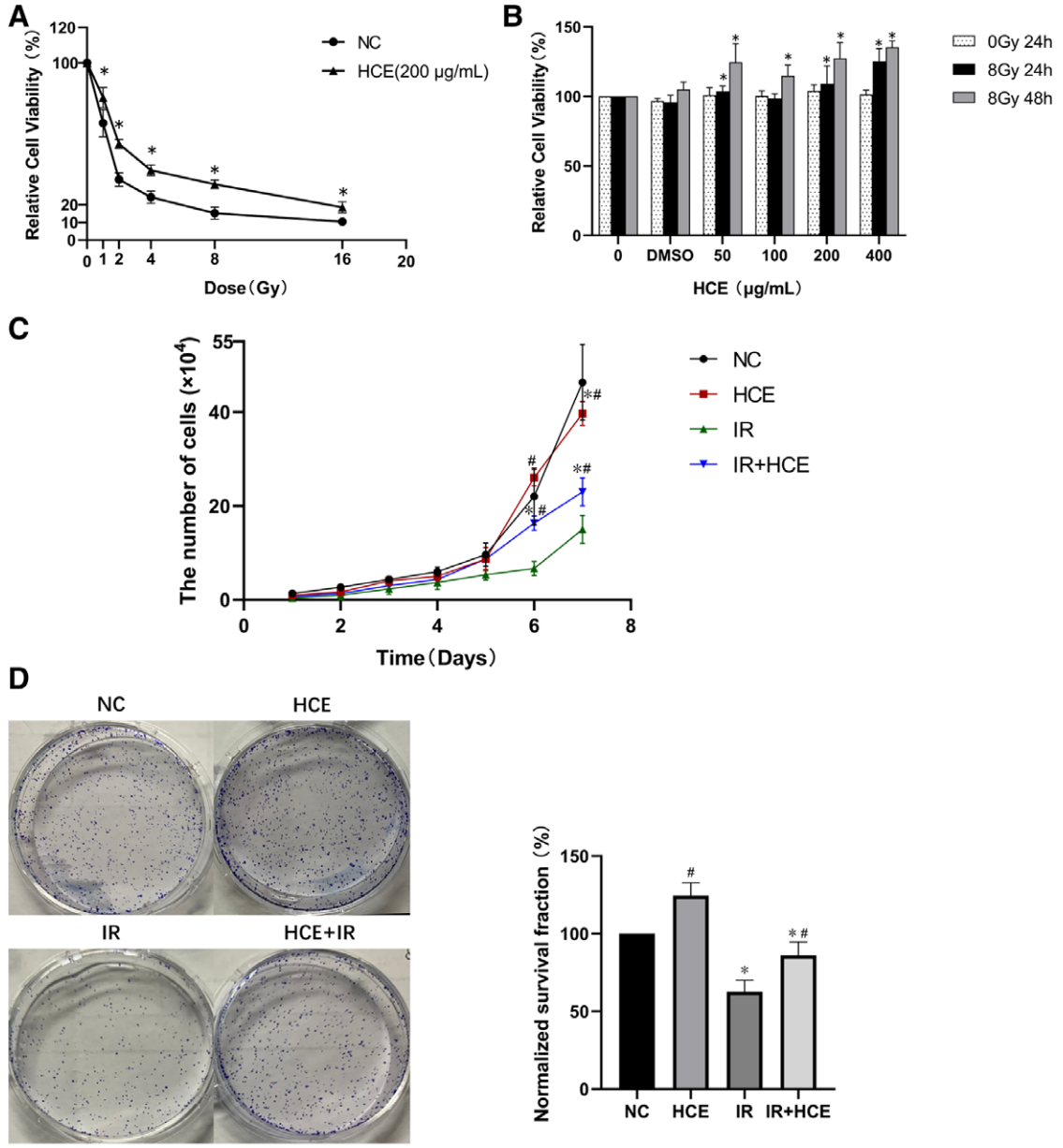

Figure 1. HCE mitigates radiation-induced damage to LO2 cells. (A) Cell viability was measured 24 h after radiation exposure at various doses (0, 1, 2, 4, 8, and 16 Gy). (B) After exposure to 8 Gy radiation, cell viability was assessed 24 and 48 h later with the addition of different concentrations of HCE. (C) Cell growth curve. (D) Clone formation experiments. Data represent the mean ± SD of three independent samples. Comparison with the NC group, $^{*}P < 0.05$,comparison with the IR group, $^{\#}P < 0.05$. HCE: *Hemerocallis citrina* extracts; IR: Ionizing radiation; NC: Negative control; SD: Standard deviation.

shows that DMSO and different concentrations of HCE (50, 100, 200, and 400 μg/mL) did not have any significant toxic effects on cell survival after irradiation. Figure 1C shows that the IR group exhibited a significant reduction in cell number and proliferation capacity compared with the NC group. Moreover, the proliferation capacity of the HCE group was slightly lower than that of the NC group, whereas the HCE + IR group showed a significantly higher proliferation capacity than the IR group. Figure 1D depicts the results of the clone formation experiments, which indicated that the HCE group had a slightly higher clone count than the NC group. Conversely, the IR and IR + HCE groups exhibited significantly reduced clone counts. Furthermore, the IR + HCE group demonstrated a significantly higher clone formation rate than the IR group. Subsequent experiments utilized a working concentration of 200 μg/mL HCE with a 24-hour exposure time.

Impact of HCE on cellular oxidative stress

To evaluate the influence of HCE on cellular oxidative stress, several markers were measured, including ROS levels (Figure 2A), MDA content (reflecting lipid peroxidation), and the activities of the endogenous antioxidants SOD and GSH (Figure 2B). The results indicated that the IR group showed significantly increased ROS levels and MDA content compared with the NC group. Conversely, HCE significantly decreased radiation-induced elevations in ROS and MDA expression. In contrast, SOD and GSH activities decreased following radiation exposure, whereas HCE significantly enhanced their activities. ROS within cells can affect mitochondria, causing a decrease in mitochondrial membrane potential and leading to mitochondrial damage, a characteristic of early apoptosis[30]. Measurements of the mitochondrial membrane potential (Figure 2C) revealed that the IR group exhibited a

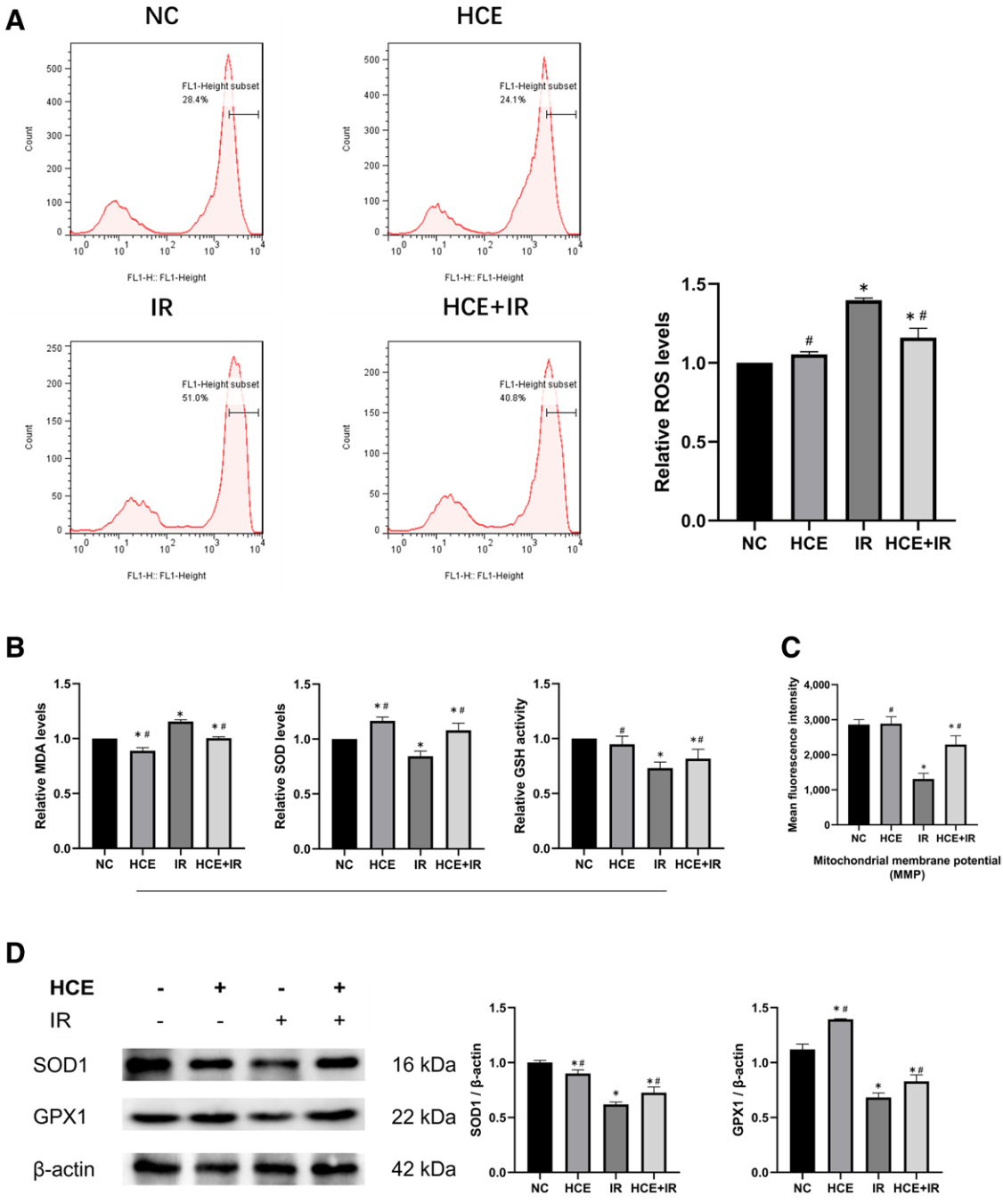

Figure 2. HCE mitigates radiation-induced oxidative stress damage in LO2 cells. Detection of ROS levels in LO2 cells (A); measurement of MDA, GSH, and SOD levels in LO2 cells (B); assessment of mitochondrial membrane potential in LO2 cells (C); Western blot analysis of SOD1 and GPX1 protein expression (D). Data represent the mean ± SD of three independent samples. Comparison with the NC group, $^{*}P < 0.05$,comparison with the IR group, $^{\#}P < 0.05$. GSH: Glutathione; HCE: *Hemerocallis citrina* extracts; IR: Ionizing radiation; MDA: Malondialdehyde; NC: Negative control; ROS: Reactive oxygen species; SD: Standard deviation; SOD: Superoxide dismutase.

significantly lower membrane potential than the NC group, which was alleviated by HCE. Additionally, the protein expression levels of SOD1 and GPX1 (Figure 2D) were evaluated. SOD1, the predominant intracellular SOD subtype, is a crucial antioxidant enzyme[31]. GPX1, a significant member of the GSH family, is one of the most abundant enzymes[32]. Alterations in the protein levels of SOD1 and GPX1 correspond to changes in SOD and GSH activities. These data suggest that HCE augment the activity of antioxidant enzymes and the expression of proteins in LO2 cells, indicating its antioxidative role in mitigating radiation-induced damage.

Impact of HCE on apoptosis and cell cycle

To further explore the potential mechanisms underlying the protective effects of HCE, flow cytometry was used to evaluate the effect of HCE on apoptosis in LO2 cells 24 h after radiation exposure. As illustrated in Figure 3A, the apoptosis rate was markedly increased in the IR group, whereas cells treated with HCE demonstrated a significant reduction in the apoptosis rate. As shown in Figure 3B, IR-induced cell cycle arrest in the G2/M phase, inhibiting DNA replication and cell division. However, the addition of HCE effectively alleviated this effect. The levels of several apoptosis-related

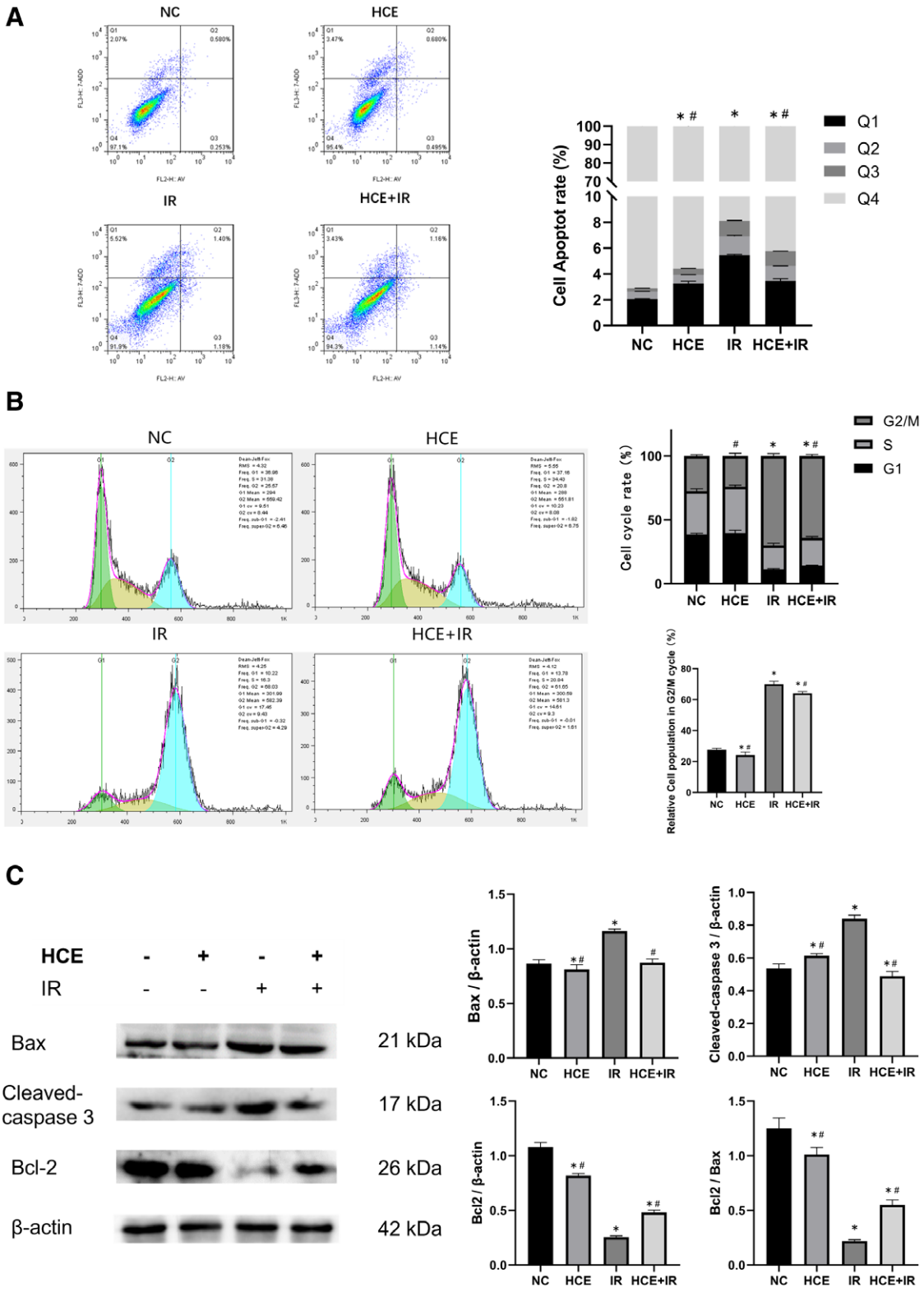

Figure 3. HCE mitigates the apoptotic effect induced by radiation in LO2 cells. Flow cytometry analysis of apoptosis in different groups (A); cell cycle analysis (B); Western blot analysis of apoptosis-related protein expression (Bax, cleaved-caspase 3, and Bcl-2) (C). Data represent the mean ± SD of three independent samples. Comparison with the NC group, $^{*}P < 0.05$,comparison with the IR group, $^{\#}P < 0.05$. HCE: Hemerocallis citrina extracts; IR: Ionizing radiation; NC: Negative control; SD: Standard deviation.

proteins, including Bcl2, Bax, and Cleaved-caspase 3 (Figure 3C), were examined to confirm the anti-apoptotic effects of HCE. However, compared with the IR group, the IR + HCE group demonstrated a decrease in Bax and Cleaved-caspase 3 protein levels and an increase in Bcl2 expression, indicating that pretreatment with HCE mitigated this apoptotic effect. The flow cytometry results were consistent with the western blot results.

Impact of HCE on cellular ferroptosis after radiation

We assessed the cellular iron death–related indices. Figure 4A shows that the addition of an iron-death

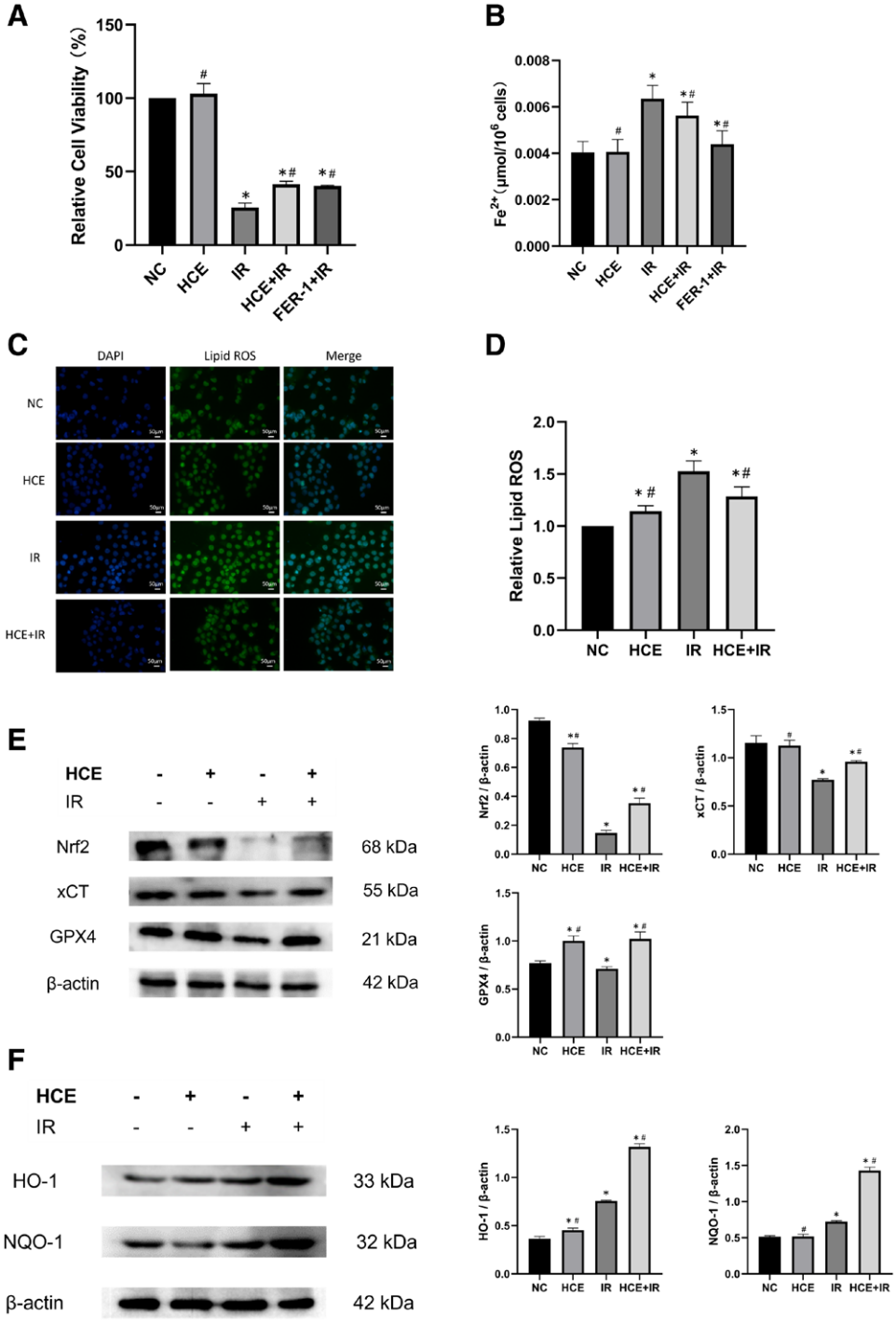

Figure 4. HCE alleviates iron-induced cell death in LO2 cells exposed to radiation. Cell viability detected using MTT assay (A); detection of cellular iron ions (B); lipid peroxidation was determined using liperfluo (C); detection of cellular lipid peroxidation (D); Western blot analysis of Nrf2, xCT, and GPX4 protein expression (E); Western blot analysis of downstream Nrf2 proteins (HO-1 and NQO-1) expression (F). Data represent the mean ± SD of three independent samples. Comparison with the NC group, $^{*}P < 0.05$,comparison with the IR group, $^{\#}P < 0.05$. HCE: Hemerocallis citrina extracts; HO-1: Heme oxygenase 1; IR: Ionizing radiation; MTT: 3-(4,5-dimethylthiazol-2-yl)-2,5-diphenyltetrazolium bromide; NC: Negative control; NQO-1: NAD(P)H quinone oxidoreductase; Nrf2: Nuclear factor erythroid 2–related factor 2; SD: Standard deviation.

inhibitor effectively mitigated the inhibitory effects on the proliferation of irradiated cells. In Figure 4B–D, the intracellular iron ion levels and lipid ROS in LO2 cells significantly increased at an 8 Gy irradiation dose, with a statistically significant difference observed. However, this increase was markedly attenuated in the HCE and FER-1 groups. As mentioned previously, HCE potentially inhibits iron-dependent cell death induced by IR in LO2 cells. To investigate the underlying mechanisms, we analyzed the expression of key proteins involved in iron-mediated cell death following IR. xCT and GPX4 proteins serve as classic suppressors of iron-dependent cell death. As depicted in Figure 4E, the expression of xCT and GPX4 was significantly increased in the IR + HCE group compared with the IR group, indicating that HCE confers cellular protection against IR-induced ferroptosis by upregulating the expression of xCT and GPX4.

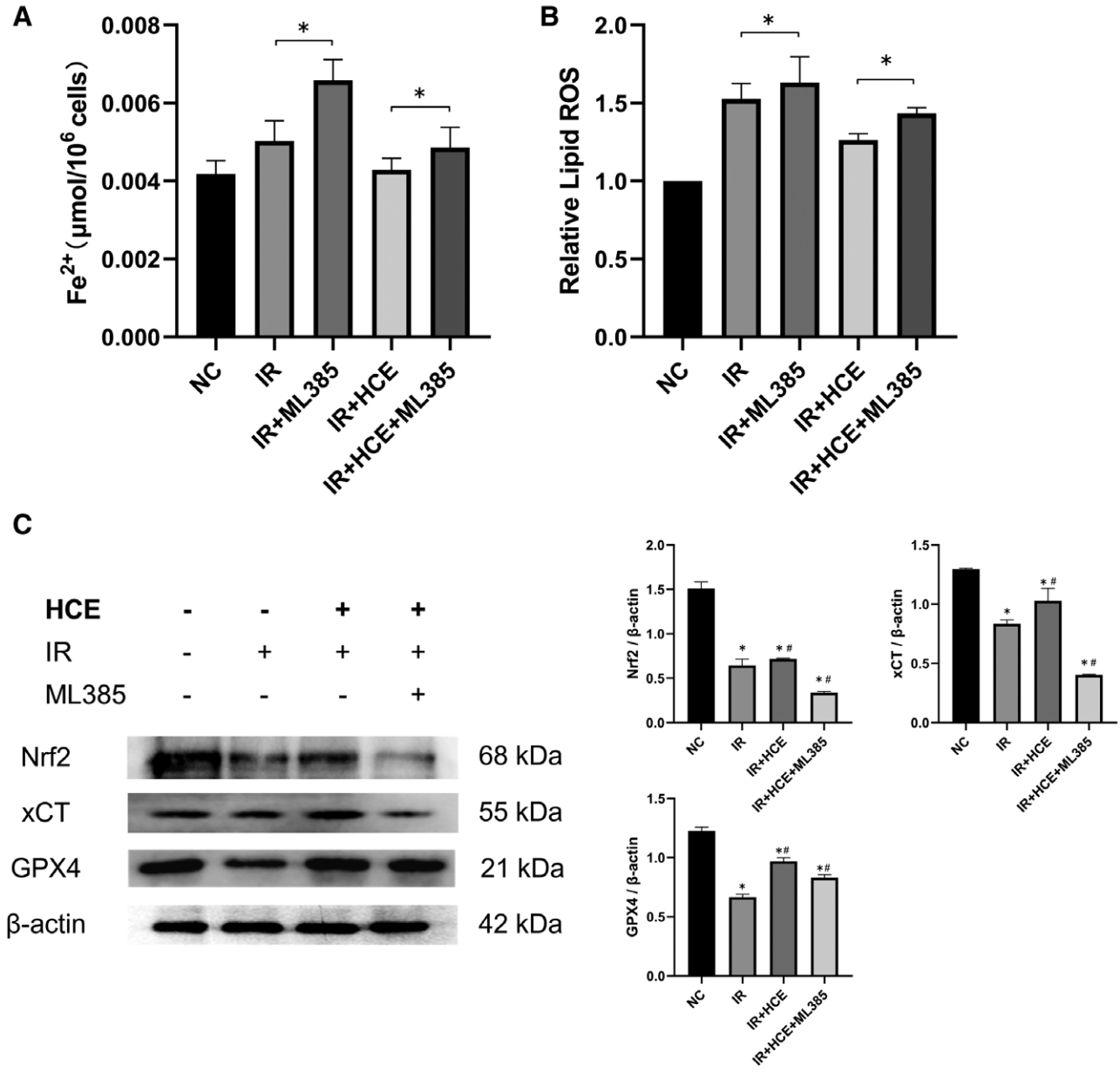

Figure 5. The addition of the Nrf2 inhibitor ML385 diminishes the protective effect of HCE on IR-induced ferroptosis in LO2 cells. Detection of cellular iron ions (A); detection of cellular lipid peroxidation (B); Western blot analysis of Nrf2, xCT, and GPX4 protein expression (C). Data represent the mean ± SD of three independent samples. Comparison with the NC group, $^{*}P < 0.05$,comparison with the IR group, $^{\#}P < 0.05$. HCE: Hemerocallis citrina extracts; IR: Ionizing radiation; NC: Negative control; Nrf2: Nuclear factor erythroid 2–related factor 2; SD: Standard deviation.

Heme oxygenase-1 (HO-1) and NQO-1 represent phase II detoxifying enzymes downstream of Nrf2 and serve as crucial defense factors in antioxidation[33]. Therefore, we postulate that HCE can upregulate these two widely expressed downstream enzymes of Nrf2, thereby conferring antioxidative protection. The protein levels of HO-1 and NQO-1 were quantified. As illustrated in Figure 4F, the results demonstrated an elevation in the expression of HO-1 and NQO-1 in the IR group. Furthermore, the expression of HO-1 and NQO-1 was further upregulated in the HCE group compared to the IR group. These findings indicate that HCE induces the expression of HO-1 and NQO-1.

Impact of HCE on ferroptosis after adding the Nrf2 inhibitor ML385

We propose that HCE regulates xCT and GPX4 through the Nrf2-xCT/GPX4 pathway, thereby influencing cellular ferroptosis. To investigate this, we added the Nrf2 inhibitor ML385 and examined the relevant indicators in LO2 cells. As shown in Figure 5A, B, in the group treated with ML385, the cellular iron ion concentration and lipid peroxidation levels increased. This indicates that HCE can modulate the downstream proteins through the Nrf2 pathway. Additionally, we evaluated the protein expression of Nrf2, xCT, and GPX4 (Figure 5C). These results indicate that when Nrf2 expression is inhibited, the expression of xCT and GPX4 proteins decreases. Therefore, HCE may protect cells from IR-induced ferroptosis by promoting Nrf2 expression and subsequently increasing xCT transcription and expression.

Discussion

Liver cancer is a malignant tumor with high morbidity and mortality rates. Globally, liver cancer has a high mortality rate owing to inadequate early detection

and treatment protocols. Consequently, most liver cancers are diagnosed in advanced stages, posing significant challenges in treatment. Numerous treatment modalities are available for liver cancer, and radiotherapy has been extensively used as a subject of considerable research interest. A focal point of research is the dual effect of IR, which not only eliminates cancer cells but also damages the surrounding normal cells. Thus, there is a critical need to explore novel radiation-protective drugs with minimal side effects and optimal efficacy.

HCE primarily contains rutin, quercetin 3-glucoside, populin, kaempferol 3-glucoranoside, quercetin, apigenin, kaempferol, among others[34]. Multiple studies have demonstrated the antioxidant, anti-radiation, and anti-iron death effects of kaempferol and quercetin. Kaempferol protects against gamma radiation–induced mortality and damage[35–37], and quercetin mitigates radiation-induced intestinal injury *via* Nrf2[38,39]. We hypothesized that HCE might possess protective effects against radiation. This study aimed to examine the impact of HCE on LO2 cells after irradiation and elucidate the specific mechanisms through which HCE exerts its effects. Our findings indicate that HCE reduces apoptosis in irradiated LO2 cells by modulating oxidative stress and related processes. Additionally, we investigated ferroptosis markers and observed a mitigating effect in the IR + HCE group, thus supporting our hypothesis. In conclusion, we propose that HCE exerts protective effects against radiation by influencing apoptosis and ferroptosis.

Our study revealed that IR decreased the proliferation rate of LO2 cells, whereas HCE effectively enhanced the proliferation rate of LO2 cells after irradiation. We speculated that this effect may be attributed to the protective nature of HCE or its influence on cellular nutritional factors. HCE did not exhibit significant cytotoxicity or promote cell growth, which was more pronounced after exposure to IR. We conducted further experiments to explore whether other factors contributed to this protective effect.

Based on our initial hypothesis, we proposed that HCE protects irradiated cells by influencing apoptosis. Apoptosis is a controlled process regulated by genes, and the expression of apoptosis-related proteins determines whether cells undergo apoptosis[40]. Studies have indicated that IR can induce apoptosis by inhibiting or enhancing the expression of apoptosis-related proteins[41]. However, flavonoids have also been reported to reduce cellular apoptosis[42].

In our study, we observed that IR led to an increase in ROS and MDA levels while reducing SOD and GPX levels in LO2 cells. However, the addition of HCE reversed these effects, indicating its antioxidative properties in irradiated LO2 cells. Further investigation revealed that HCE reduced the rate of apoptosis in LO2 cells after irradiation. In the HCE + IR group, the expression of the anti-apoptotic protein Bcl2 increased, whereas that of the pro-apoptotic proteins Bax and Cleaved-caspase 3 decreased. These findings suggest that HCE exerts an anti-apoptotic effect on irradiated LO2 cells.

Ferroptosis is a form of non-apoptotic cell death triggered by metabolic stress, such as the depletion of GSH[43]. Recent studies have indicated that xCT overexpression can inhibit ferroptosis by facilitating cysteine import, promoting GSH biosynthesis, and aiding the detoxification of lipid peroxides by GPX4. Subsequently, we investigated the expression levels of key proteins involved in ferroptosis. Our findings revealed that HCE effectively enhanced the expression of xCT and GPX4 in LO2 cells. This suggests that HCE regulates IR-induced apoptosis and ferroptosis in LO2 cells by modulating xCT expression. Furthermore, xCT overexpression diminished lipid ROS and IR-induced cell death. Therefore, we hypothesized that HCE regulated ferroptosis in LO2 cells by interacting with xCT.

Studies have indicated that Nrf2 exerts its antioxidative effects on cellular protection by regulating xCT expression[44]. Therefore, we hypothesized that HCE regulates xCT expression by modulating Nrf2. The addition of an Nrf2 inhibitor significantly reduced the expression of xCT and GPX4. Further investigations revealed that the downregulation of Nrf2 expression also affects oxidative stress in LO2 cells. For example, the expression of the anti-apoptotic protein Bcl2 decreases, whereas the levels of the pro-apoptotic proteins Bax and Cleaved-caspase 3 increase. Furthermore, Nrf2 overexpression mitigates lipid ROS- and IR-induced cell death. Consistent with previous reports, HCE can regulate the expression of Nrf2 by modulating its stability[43]. Nrf2 also regulates the transcriptional activity of xCT. In summary, our study suggests that HCE attenuates radiation-induced LO2 cell damage *via* the Nrf2-xCT/GPX4 signaling pathway. These findings suggest that HCE effectively attenuates apoptosis and ferroptosis in LO2 cells following irradiation, offering new possibilities for the future development of enhanced radiation protection agents.

Conclusions

In conclusion, HCE demonstrates protective effects against radiation-induced oxidative stress, apoptosis, and ferroptosis in cells. These protective effects are mediated by activation of the Nrf2 pathway and its downstream antioxidant factors, including HO-1 and NQO-1. Moreover, HCE attenuates radiation-induced ferroptosis *via* the Nrf2-xCT/GPX4 pathway. The findings of this study provide a theoretical foundation for the radioprotective effect of HCE on LO2 cells and offer a novel perspective on the utilization of Chinese herbal medicine for radiation protection.

Conflict of interest statement

The authors declare no conflict of interest.

Funding

This work was supported by the Natural Science Foundation of Hunan Province (2021JJ30592), Health Commission Scientific Research Project of Hunan Province (D202309037942), Key Research Project of

Education Department of Hunan Province (19A429), and National Natural Science Foundation of China (81272994).

Author contributions

Zihao Zhu and Yan Wang were the main researchers of this study, taking charge of conducting experiments, collecting data, and writing research manuscripts. Qi Liu and Zhengzheng Deng aided in the research efforts, while Qiancheng Qing and Pengyuan Lei provided assistance with statistical analyses of the research data. Jinjing Guo contributed to data management. Bo Huang conceptualized the research objectives, designed methods, supervised and funded the project. All authors reviewed and edited the final manuscript.

Ethical approval of studies and informed consent

Not applicable.

Acknowledgments

None.

Data availability

All relevant data are within the manuscript.

References

[1] Akiyama M. Late effects of radiation on the human immune system: an overview of immune response among the atomic-bomb survivors. *Int J Radiat Biol* 1995;68(5):497–508.
[2] Hymes SR, Strom EA, Fife C. Radiation dermatitis: clinical presentation, pathophysiology, and treatment 2006. *J Am Acad Dermatol* 2006;54(1):28–46.
[3] McQuestion M. Evidence-based skin care management in radiation therapy. *Semin Oncol Nurs* 2006;22(3):163–173.
[4] Ryan JL. Ionizing radiation: the good, the bad, and the ugly. *J Invest Dermatol* 2012;132(3 Pt 2):985–993.
[5] Li T, Cao Y, Li B, et al. The biological effects of radiation-induced liver damage and its natural protective medicine. *Prog Biophys Mol Biol* 2021;167:87–95.
[6] Baidoo KE, Yong K, Brechbiel MW. Molecular pathways: targeted α-particle radiation therapy. *Clin Cancer Res* 2013;19(3):530–537.
[7] Dixon SJ, Lemberg KM, Lamprecht MR, et al. Ferroptosis: an iron-dependent form of nonapoptotic cell death. *Cell* 2012;149(5):1060–1072.
[8] Doll S, Proneth B, Tyurina YY, et al. ACSL4 dictates ferroptosis sensitivity by shaping cellular lipid composition. *Nat Chem Biol* 2017;13(1):91–98.
[9] Stockwell BR, Friedmann Angeli JP, Bayir H, et al. Ferroptosis: a regulated cell death nexus linking metabolism, redox biology, and disease. *Cell* 2017;171(2):273–285.
[10] Hu CL, Nydes M, Shanley KL, et al. Reduced expression of the ferroptosis inhibitor glutathione peroxidase-4 in multiple sclerosis and experimental autoimmune encephalomyelitis. *J Neurochem* 2019;148(3):426–439.
[11] Torti SV, Torti FM. Iron and cancer: more ore to be mined. *Nat Rev Cancer* 2013;13(5):342–355.
[12] Lang X, Green MD, Wang W, et al. Radiotherapy and immunotherapy promote tumoral lipid oxidation and ferroptosis via synergistic repression of SLC7A11. *Cancer Discov* 2019;9(12):1673–1685.
[13] Hashem S, Ali TA, Akhtar S, et al. Targeting cancer signaling pathways by natural products: exploring promising anti-cancer agents. *Biomed Pharmacother* 2022;150:113054.
[14] Ferreyra MLF, Serra P, Casati P. Recent advances on the roles of flavonoids as plant protective molecules after UV and high light exposure. *Physiol Plant* 2021;173(3):736–749.
[15] Kashyap D, Garg VK, Tuli HS, et al. Fisetin and quercetin: promising flavonoids with chemopreventive potential. *Biomolecules* 2019;9(5):174.
[16] Badshah SL, Faisal S, Muhammad A, et al. Antiviral activities of flavonoids. *Biomed Pharmacother* 2021;140:111596.
[17] Fan ZL, Wang ZY, Zuo LL, et al. Protective effect of anthocyanins from lingonberry on radiation-induced damages. *Int J Environ Res Public Health* 2012;9(12):4732–4743.
[18] Wang C, Yu S, Jiang J, et al. Protective effect of anthocyanins on radiation-induced hippocampal injury through activation of SIRT3. *Curr Pharm Des* 2022;28(13):1103–1108.
[19] Matraszek-Gawron R, Chwil M, Terlecka P, et al. Recent studies on anti-depressant bioactive substances in selected species from the genera hemerocallis and gladiolus: a systematic review. *Pharmaceuticals (Basel)* 2019;12(4):172.
[20] Que F, Mao L, Zheng X. In vitro and vivo antioxidant activities of daylily flowers and the involvement of phenolic compounds. *Asia Pac J Clin Nutr* 2007;16(Suppl 1):196–203.
[21] Sang T, Fu YJ, Song L. Polysaccharides from Hemerocallis citrina Baroni inhibit the growth of hepatocellular carcinoma cells by regulating the Wnt/β-catenin pathway. *Nutr Cancer* 2023;75(8):1658–1672.
[22] Moi P, Chan K, Asunis I, et al. Isolation of NF-E2-related factor 2 (Nrf2), a NF-E2-like basic leucine zipper transcriptional activator that binds to the tandem NF-E2/AP1 repeat of the beta-globin locus control region. *Proc Natl Acad Sci USA* 1994;91(21):9926–9930.
[23] Sengoku T, Shiina M, Suzuki K, et al. Structural basis of transcription regulation by CNC family transcription factor, Nrf2. *Nucleic Acids Res* 2022;50(21):12543–12557.
[24] Anuranjani, Bala M. Concerted action of Nrf2-ARE pathway, MRN complex, HMGB1 and inflammatory cytokines—implication in modification of radiation damage. *Redox Biol* 2014;2:832–846.
[25] Cruz-Gregorio A, Aranda-Rivera AK, Pedraza-Chaverri J. Nuclear factor erythroid 2-related factor 2 in human papillomavirus-related cancers. *Rev Med Virol* 2022;32(3):e2308.
[26] Dong H, Qiang Z, Chai D, et al. Nrf2 inhibits ferroptosis and protects against acute lung injury due to intestinal ischemia reperfusion via regulating SLC7A11 and HO-1. *Aging (Milano)* 2020;12(13):12943–12959.
[27] Yamaguchi I, Yoshimura SH, Katoh H. High cell density increases glioblastoma cell viability under glucose deprivation via degradation of the cystine/glutamate transporter xCT (SLC7A11). *J Biol Chem* 2020;295(20):6936–6945.
[28] Rabinowitz J, Sharifi HJ, Martin H, et al. xCT/SLC7A11 antiporter function inhibits HIV-1 infection. *Virology* 2021;556:149–160.
[29] Jiang N, Zhang Y, Yao C, et al. Hemerocallis citrina Baroni ameliorates chronic sleep deprivation-induced cognitive deficits and depressive-like behaviours in mice. *Life Sci Space Res* 2024;40:35–43.
[30] Jia Y, Han Y, Wang X, et al. Role of apoptosis in the Post-traumatic stress disorder model-single prolonged stressed rats. *Psychoneuroendocrinology* 2018;95:97–105.
[31] Hwang J, Jin J, Jeon S, et al. SOD1 suppresses pro-inflammatory immune responses by protecting against oxidative stress in colitis. *Redox Biol* 2020;37:101760.
[32] Espinosa-Diez C, Miguel V, Mennerich D, et al. Antioxidant responses and cellular adjustments to oxidative stress. *Redox Biol* 2015;6:183–197.
[33] Sun Y, Yang T, Mao L, et al. Sulforaphane protects against brain diseases: roles of cytoprotective enzymes. *Austin J Cerebrovasc Dis Stroke* 2017;4(1):1054.
[34] Li S, Cui H, Wang J, et al. Qualitative and quantitative analysis on flavonoid distribution in different floral parts of 42 hemerocallis accessions. *Front Plant Sci* 2021;12:670506.
[35] Wang J, Li T, Feng J, et al. Kaempferol protects against gamma radiation-induced mortality and damage *via* inhibiting oxidative stress and modulating apoptotic molecules *in vivo* and *vitro*. *Environ Toxicol Pharmacol* 2018;60:128–137.
[36] Yao K, Chen H, Liu K, et al. Kaempferol targets RSK2 and MSK1 to suppress UV radiation-induced skin cancer. *Cancer Prev Res (Phila)* 2014;7(9):958–967.
[37] Yuan Y, Zhai Y, Chen J, et al. Kaempferol ameliorates oxygen-glucose deprivation/reoxygenation-induced neuronal ferroptosis by activating Nrf2/SLC7A11/GPX4 axis. *Biomolecules* 2021;11(7):923.

[38] Cui Z, Zhao X, Amevor FK, et al. Therapeutic application of quercetin in aging-related diseases: SIRT1 as a potential mechanism. *Front Immunol* 2022;13:943321.
[39] Zhu X, Li Y, Yue L, et al. Quercetin mitigates radiation-induced intestinal injury and promotes intestinal regeneration via Nrf2-mediated antioxidant pathway1. *Radiat Res* 2023;199(3):252–262.
[40] D'Arcy MS. Cell death: a review of the major forms of apoptosis, necrosis and autophagy. *Cell Biol Int* 2019;43(6):582–592.
[41] Vitale I, Pietrocola F, Guilbaud E, et al. Apoptotic cell death in disease-current understanding of the NCCD 2023. *Cell Death Differ* 2023;30(5):1097–1154.
[42] Abusaliya A, Jeong SH, Bhosale PB, et al. Mechanistic action of cell cycle arrest and intrinsic apoptosis via inhibiting Akt/mTOR and activation of p38-MAPK signaling pathways in Hep3B liver cancer cells by prunetrin-A flavonoid with therapeutic potential. *Nutrients* 2023;15(15):3407.
[43] Feng H, Liu Y, Gan Y, et al. AdipoR1 regulates ionizing radiation-induced ferroptosis in HCC cells through Nrf2/xCT pathway. *Oxid Med Cell Longevity* 2022;2022:8091464.
[44] Li X, Zhan J, Hou Y, et al. Coenzyme Q10 suppresses oxidative stress and apoptosis *via* activating the Nrf-2/NQO-1 and NF-κB signaling pathway after spinal cord injury in rats. *Am J Transl Res* 2019;11(10):6544–6552.